Novel high performance poly(p-phenylene benzobisimidazole) (PBDI) membranes fabricated by interfacial polymerization for H 2 separation

Shan, Meixia; Liu, Xinlei; Wang, Xuerui; Liu, Zilong; Iziyi, Hodayfa; Ganapathy, Swapna; Gascon, Jorge; Kapteijn, Freek

DOI
10.1039/c9ta01524h

Publication date
2019

Document Version
Accepted author manuscript

Published in
Journal of Materials Chemistry A

Journal of
Materials Chemistry A

Accepted Manuscript

This article can be cited before page numbers have been issued, to do this please use: M. Shan, X. Liu, X. Wang, Z. Liu, H. Iziyi, S. Ganapathy, J. Gascon and F. Kapteijn, *J. Mater. Chem. A*, 2019, DOI: 10.1039/C9TA01524H.

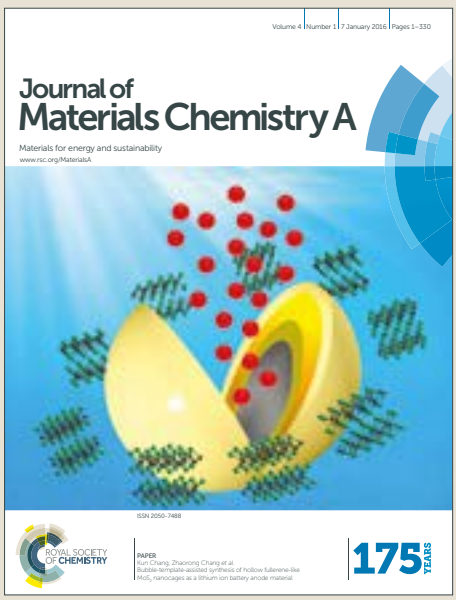

ROYAL SOCIETY OF CHEMISTRY

rsc.li/materials-a

View Article Online
DOI: 10.1039/C9TA01524H

Journal Name

ARTICLE

Novel high performance poly(p-phenylene benzobisimidazole) (PBDI) membranes fabricated by interfacial polymerization for H_2 separation

Received 00th January 20xx,
Accepted 00th January 20xx

DOI: 10.1039/x0xx00000x

www.rsc.org/

Meixia Shan[a], Xinlei Liu[a*], Xuerui Wang[a], Zilong Liu[b], Hodayfa Iziyi[a], Swapna Ganapathy[c], Jorge Gascon[a,d] and Freek Kapteijn[a*]

Membranes with high selectivity and permeance are needed to reduce the energy consumption in hydrogen purification and pre-combustion CO_2 capture. Polybenzimidazole (PBI) is one of the leading membrane materials for this separation. In this study, we present superior novel supported PBI (poly(p-phenylene benzobisimidazole, PBDI) membranes prepared by a facile interfacial polymerization (IP) method. The effect of IP reaction duration, operating temperature and pressure on membrane separation performance was systematically investigated. The best performance was achieved for membranes prepared in 2 h reaction time. The resulting membranes display an ultrahigh mixed-gas H_2/CO_2 selectivity of 23 at 423 K together with an excellent H_2 permeance of 241 GPU, surpassing the membrane performance of conventional polymers (the 2008 Robeson upper bound). These separation results, together with the facile manufacture, pressure resistance, long-term thermostability (> 200 h) and economic analysis, recommend the PBDI membranes for industrial use in H_2 purification and pre-combustion CO_2 capture. Besides, PBDI membranes possesss high selectivities towards H_2/N_2 (up to 60) and H_2/CH_4 (up to 48) mixtures, indicating their potential applications in ammonia synthesis and syngas production.

1. Introduction

The consumption of fossil fuels has brought a variety of environmental issues. Hydrogen holds great potential as an alternative fuel because of its high combustion heat and zero-carbon emission (only water as product). [1, 2] Besides, H_2 is also widely used in the chemical industry for hydrogenation reactions,[3] methanol and ammonia production,[4] which makes it an important commodity. Currently, approximately 80 % of the hydrogen is produced by natural gas and petroleum reforming.[5] Production of H_2 through abundant coal or biomass via gasification is also a viable alternative.[6] However, the main by-product of these processes is CO_2, which is a major environmental concern due to its accompanying greenhouse effect. Thus, H_2 purification by capturing CO_2 is drawing a lot of attention**.** Further, recovery of valuable H_2 from industrial vent gases and adjusting $H_2/CO\text{-}CO_2$ ratio in syngas are important industrial activities. The current technologies for hydrogen purification, such as scrubbing technology, pressure swing adsorption and cryogenic distillation are highly energy and capital intensive.[7] Membranes that are H_2-permeating and CO_2-rejecting at syngas operating conditions (423 K and above) would provide a low-cost and energy-efficient routes for H_2 purification and CO_2 capture.[8-12]

Inorganic membranes, such as palladium,[13] zeolites,[14] graphene oxide (GO),[15] and metal organic frameworks (MOFs) [16, 17] have exhibited outstanding selectivity or permeance for H_2/CO_2 separation. However, high production costs, mechanical brittleness and the fabrication complexities make these inorganic membranes less commercially attractive. In addition, engineering these materials into thin membranes and on a large-scale is extremely challenging. Polymer membranes, on the other hand, are economically acceptable, easy to process and able to produce on a large scale.[18]

Gas permeation through a dense polymer membrane generally follows the solution-diffusion mechanism,[19] where gas permeability (P) is determined by both gas solubility (S) and diffusivity (D) ($P = S \times D$). The smaller H_2 molecule and the higher solubility of CO_2 result in an opposite trend in diffusivity and solubility selectivities, thus conventional polymer membranes usually have moderate H_2/CO_2 selectivity. For example, the commercial cellulose, polysulfone and Matrimid® polymers only show an H_2/CO_2 selectivity around 3 at 308 K.[20,21] In addition, the main drawback of polymeric membranes for H_2/CO_2 separation is the lack of thermochemical stability at syngas operating conditions.

[a] Catalysis Engineering, Chemical Engineering Department, Delft University of Technology, Van der Maasweg 9, 2629 HZ Delft, The Netherlands
*Emails: x.liu-8@tudelft.nl; f.kapteijn@tudelft.nl
[b] Organic Materials & Interface, Chemical Engineering, Delft University of Technology, Van der Maasweg 9, 2629 HZ Delft, The Netherlands
[c] Department of Radiation Science and Technology, Delft University of Technology, Mekelweg 15, 2629 JB Delft, The Netherlands
[d] King Abdullah University of Science and Technology, KAUST Catalysis Center, Advanced Catalytic Materials. Thuwal 23955, Saudi Arabia
Electronic Supplementary Information (ESI) available.

DOI: 10.1039/C9TA01524H

Polybenzimidazoles (PBI),[22] are a class of heterocyclic polymers that can meet the syngas separation requirements in theory because of their exceptional thermal and chemical stability and high intrinsic H_2/CO_2 selectivity.[23] Unfortunately, PBI membrane exhibits very low H_2 permeability owing to the microstructural rigidity and tightly chain packing. Several approaches have been taken to enhance PBI membrane permeability including polymer blending,[24] structural modification,[25, 26] chemical cross-linking,[27, 28] thermal rearrangement[29] and incorporation of fillers.[2, 30, 31] Besides free-standing PBI membranes, asymmetric PBI membranes in the configuration of flat sheets and hollow fibers[8, 25, 30, 32] have been unveiled, prepared by phase inversion. Despite great achievements made in the development of thin PBI membranes, coating of an additional layer of silicone rubber was always applied to heal the defects and compensate the low processability of PBI.[33] In this sense, the development of novel PBI membrane materials and approaches for membrane fabrication are still highly on demand.

Interfacial polymerization (IP) is a commercially common, well adapted technique for the synthesis of large-scale and ultrathin polyamide membranes for reverse osmosis and nanofilitration.[34-37] Despite IP approach has been used in industry, it remains largely unexplored for preparing other polymeric membranes, such as PBI membranes. PBI was generally synthesized either by the coupling of phenylenediamines and carboxylic acids under strong acidic conditions and high temperatures or through the condensation reaction of phenylenediamines and aldehydes using some oxidative reagents,[38] resulting in intractable powders, which are nearly insoluble in common organic solvents, restricting their further processing into membranes.

In this work, we demonstrate the feasibility for fabricating thin novel PBI films and membranes on the basis of poly(*p*-phenylene benzobisimidazole (PBDI) materials,[39, 40] by using a room temperature IP protocol. The resulting membranes have been tested for H_2/CO_2 separation over a wide range of temperatures. In addition, the influence of reacting duration, feed pressures, operating temperature and other gases (N_2 and CH_4) on the membrane performance have also been investigated. As far as we know, this is the first report of using IP method for creating thin PBDI membranes with ultrahigh H_2 separation performance (H_2 permeance up to 241 GPU together with high H_2/CO_2 selectivity of 23 at 423 K).

2. Experimental

2.1 Materials

Terephthalaldehyde (TPA) (99%), 1,2,4,5-Benzenetetramine tetrahydrochloride (BTA), Toluene (anhydrous, 99.8%), Ethanol (95%), and N,N-Dimethylformamide (DMF, anhydrous, 99.8%) were purchased from Sigma Aldrich. Deionized water was supplied by Applied Sciences of Delft University of Technology. Asymmetric α-Al_2O_3 substrates (α-Al_2O_3, average pore size ~ 2.5 μm; γ-Al_2O_3 layer on top, average pore size ~ 5.0 nm) with a diameter of 18 mm and a thickness of 1 mm were purchased from Fraunhofer-Institut für Keramische Technologien und Systeme IKTS. All materials and solvents were used without further purification.

2.2. Synthesis of PBDI films

A TPA solution in toluene (1.0 wt.%) was gently spread on top of a 1.5 wt.% aqueous solution containing BTA in a petri dish (or bottle). After a few seconds, a brown layer was formed at the water-toluene interface. The film was left for 3 h and then washed. The resulting films were left to dry in the fume hood and finally dried under vacuum at 373 K overnight. Plenty of films were prepared in this way for later characterization.

2.3 Synthesis of supported PBDI membranes

An α-Al_2O_3 substrate was first immersed in a small clean petri dish (diameter ~ 5 cm) containing 1.5 wt.% BTA aqueous solution under reduced pressure of 0.2 bara (absolute pressure). After 20 min, the solution was taken out from the petri dish and the substrate was dried with compressed air until no visible droplets were left on the surface. The 1.0 wt.% TPA solution was then poured onto the BTA saturated α-Al_2O_3 substrate and the reaction was let to continue for 1, 2 or 3 h. The membrane was left in the fume hood overnight, washed, dried at RT and finally put into a homemade permeation setup for performance testing. The specific membrane preparation conditions are provided in Table 1. All membranes were prepared in duplicate to confirm the reproducibility (Table S1).

Table 1. Summary of membrane preparation conditions.

Membranes	Interfacial polymerization conditions		
	Aqueous amine phase (wt.%)	Aldehyde in toluene phase (wt.%)	IP time (h)
M1	1.5	1.0	1
M2	1.5	1.0	2
M3	1.5	1.0	3

2.4. Characterization

The thermostability was determined by thermogravimetric analysis (TGA) performed in a Mettler Toledo TGA/SDTA851e apparatus by measuring the mass loss of the sample while heating the sample under N_2 (100 mL·min^{-1}) from 303 to 1073 K at a heating rate of 5 K·min^{-1}.

Diffuse reflectance infrared Fourier transform spectra (DRIFTs) of the PBDI films were acquired using a Nicolet 8700 FT-IR (Thermo Scientific) equipped with a high-temperature cell with CaF_2 windows. The samples were preheated in He at 423 K for 30 min to eliminate the influence from the trapped solvents.

A Bruker-D8 advanced diffractometer with Co-K_α radiation (λ = 1.78897 Å) was used to record the powder X-ray diffraction (PXRD) patterns of PBDI films. The samples were scanned in the 2ϑ range of 5° - 80° using a scan speed of 0.2 seconds per step and a step size of 0.02° in a continuous scanning mode.

Scanning electron microscope (SEM) images of PBDI films were acquired with a JEOL JSM-6010LA InTouchScope microscope. The

surface and cross-section images of the supported membranes were obtained using a DualBeam Strata 235 microscope (FEI) and an AURIGA Compact (Zeiss) microscope. Prior to the analyses, the specimens were sputter-coated with gold.

CO_2 (273, 298 and 323 K) and N_2 (77 K) adsorption/desorption isotherms were recorded in a TriStar II 3020 (Micromeritics) instrument. Prior to the gas adsorption measurements, the samples were degassed at 423 K under N_2 flow overnight.

Atomic Force Microscopy (AFM) tomography images were acquired in tapping mode using a silicon tip (NSG03, NT-MDT), with a nominal value of the tip radius of 7 nm and a nominal spring constant of 0.4–2.7 N/m. Images were recorded over a 1 µm × 1 µm area with 512 × 512 data points, at room temperature, and at a scan rate of 1 Hz.

Solid state Nuclear Magnetic Resonance (NMR) measurements were performed using a Bruker Ascend 500 spectrometer operating at a ^{13}C frequency of 125.76 MHz and equipped with a two channel 4 mm MAS probe head (Bruker) at a 10 kHz spinning speed. One dimensional ^{13}C CP/MAS spectra were recorded, where a proton π/2 pulse length of 3 µs and a cross polarization period of 2 ms was used. 140000 scans were accumulated with a recycle delay of 5 s between scans. An exponential apodization function corresponding to a line broadening of 80 Hz was applied prior to Fourier transformation.

2.5. Gas permeation experiments

The PBDI membranes (effective area of 1.33 cm^2) were mounted in a flange between Viton® O-rings. This flange fits in a permeation module that was placed inside an oven in a home-made permeation setup.[41] The mixed gas permeation measurements were carried out using an equimolar mixture of H_2 and CO_2, N_2 or CH_4 (50 mL·min^{-1} for each gas) as feed. Helium (4.6 mL·min^{-1}) was used as sweep gas at the permeate side. The absolute pressure of the feed stream was adjusted in a range of 1 - 5 bara through a back-pressure controller at the retentate side, keeping the permeate side at atmospheric pressure. The permeation module was placed in a convection oven to control the temperature from 298 to 423 K. An on-line gas chromatograph (Interscience Compact GC) equipped with a packed Carboxen 1010 PLOT (30 m x 0.32 mm) column and TCD and FID detectors was used to analyze the gas compositions in the permeate.

Gas separation performance is defined by the selectivity (*α*) and the gas permeance (*P*) of the individual components. The permeance of component *i* (P_i) was calculated as follows (Equation 1):

$$P_i = \frac{N_i}{\Delta p_i \cdot A} = \frac{F_i}{\Delta p_i} \quad (1)$$

where N_i denotes the permeation rate of component *i* (mol s^{-1}), F_i is the molar flux of compound *i* (mol m^{-2} s^{-1}), *A* is the membrane area and Δp_i represents the partial pressure difference of component *i* across the membrane and calculated according to Equation 2.

$$\Delta p_i = p_{feed} \times Y_{i,feed} - p_{perm} \times X_{i,perm} \quad (2)$$

where p_{feed} and p_{perm} represent the pressures at the feed and permeate sides and $Y_{i,feed}$ and $X_{i,perm}$ are the molar fractions of component *i* in the feed and permeate gas streams, respectively.

The SI unit for the permeance is mol·s^{-1}·m^{-2}·Pa^{-1}. However, gas permeances are widely reported in units GPU (Gas Permeation Unit), where 1 GPU = 3.35 x 10^{-10} mol·s^{-1}·m^{-2}·Pa^{-1}.

Gas permeability is an intrinsic property of the membrane material and typically used for the evaluation of the separation performance of dense polymeric membranes. The unit of permeability is Barrer, where 1 Barrer = 3.35 x 10^{-16} mol·s^{-1}·m^{-1}·Pa^{-1}. Gas selectivity (*α*) was calculated as the ratio of the permeance of the faster permeating component (H_2 in this study) to the permeance of the less permeating component (CO_2, N_2 and CH_4 in this study). For H_2 and CO_2 as an example this reads (equation 3):

$$a_{H_2/CO_2} = \frac{P_{H_2}}{P_{CO_2}} \quad (3)$$

Ideal selectivity was applied in the case of single component data.

3. Results and discussion

3.1 Characterization

In order to study the feasibility of the IP protocol to fabricate PBDI membranes, as preliminary experiments the preparation of free-standing PBDI films was conducted at the interface of two immiscible liquid phases (Fig. 1). As depicted in Fig. 1a, a brown layer formed at the interface. The amine groups in aqueous BTA solution reacted quickly with the aldehyde moieties in toluene upon contacting. The growing film itself behaves as a barrier and confines the reaction to the remaining defects, yielding a continuous film (see Movie S1). The film surface was smooth with some spherical particles on top (Fig. 2c), attributed to emulsion droplets near the organic interface. A large number of spherical particles were observed beneath the film (Fig. 2d) because of the hydrophilicity of the PBDI.[34] The dense film layer has a thickness of around 300 nm (Fig. 2a and b).

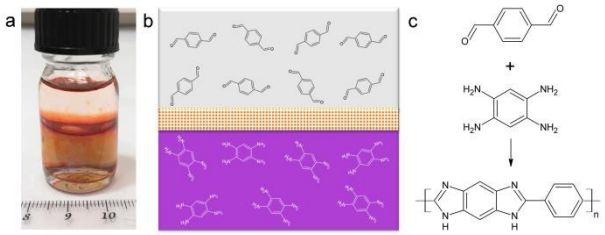

Fig. 1 (a) Photograph of a free-standing PBDI film formed at the toluene-water interface. (b) Description of PBDI film preparation procedure. The aqueous BTA solution (bottom purple area) was contacted with TFB toluene solution (upper grey part), enabling the formation of PBDI film (orange part) at the interface. (c) Reaction scheme for PBDI.

The formation of benzimidazoles was confirmed by DRIFT spectroscopy and $^{13}CP/MAS$ NMR. (Fig. 3a and b). Specifically, the C=N stretching band of the benzimidazole system in the vicinity of

View Article Online
DOI: 10.1039/C9TA01524H

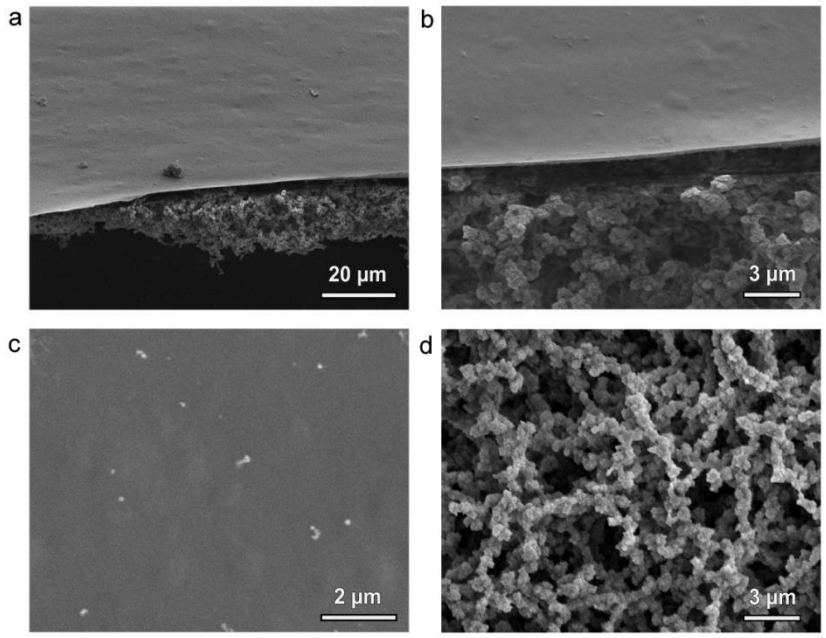

Fig. 2 Cross-sectional (a and b) and surface SEM images of a free-standing PBDI film (c, surface faced toluene phase, and d, surface faced water phase).

1616 cm^{-1} together with the skeleton vibration of benzimidazole ring at 1490, 1375, and 1240 cm^{-1} were observed. In line with the DRIFTs observations, the successful condensation between BTA and TPA units were further corroborated by ^{13}CP/MAS NMR. The full assignments of the peaks are shown in Fig. 3b. Specifically, a signal at 151 ppm corresponds to the characteristic stretching of N=C-N band in the benzimidazole ring. Additional signals at 100 and 130 ppm are characteristic of aromatic carbons, indicating the incorporation of BTA and TPA units in the network. The thermal stability of the film was evaluated by TGA. PBDI is stable up to 800 K (Fig. 3c). The slight weight loss below 390 K can be attributed to the desorption of moisture or solvent trapped in the network. The weight loss between 390 K and 640 K was caused by the decomposition of oligomer and residual monomers trapped in the network.[42]

Furthermore, the X-ray diffraction pattern of PBDI films presented in Fig. 3d reflects a diffraction pattern different from normal polybenzimidazoles. One diffraction assigned to the *d*-spacing of 0.4 nm was reported for PBI membranes[28] whereas two diffractions at 13° and 30°, corresponding to a *d*-spacing of 0.79 nm and 0.35 nm, respectively, were observed for PBDI, demonstrating a different packing of polymer chains. The two reflections of PBDI can be probably assigned to the distance of polybenzimidazole chains and the parallel orientation of benzimidazole rings with respect to the film surface.[43, 44]

In order to study the texture properties of the prepared film, low-pressure N_2 sorption measurement was performed at 77 K (Fig. 3e), The film shows a very low N_2 uptake and the isotherms are fully reversible, indicating the low accessibility of the network towards N_2, pointing at a submicroporous material. The Brunauer-Emmett-Teller area was too low to be calculated, reached the detection limit of the adsorption instrument. Furthermore, CO_2 adsorption isotherms at different temperatures (Fig. 3f) were determined to check whether diffusion limitations at 77 K could be the reason for the small N_2 uptake. The low CO_2 adsorption further confirms the dense packing structure of the PBDI film. Moreover, the Virial equation (Eq. (S1), (S2), see details in SI) was used to calculate the steric heat of CO_2 adsorption $\boldsymbol{Q_{st}}$ on PBDI, ranging from ~34 kJ mol^{-1} (Fig. S1) at low loading, which is even slightly higher than for other benzimidazole polymers,[45, 46] indicating its high binding ability towards CO_2, decreasing to ~30 kJ mol^{-1} at higher loading. Compared with the free-standing film, the membrane formed on top of the alumina support is relatively thicker, around 800 nm (Fig. 4d). It seems that the solid substrate effectively anchored the membrane, preventing the migration of PBDI oligomers to the aqueous phase and stabilizing the interface for continuous reaction. Particles with size down to 20 nm were possibly recognized on the

View Article Online
DOI: 10.1039/C9TA01524H

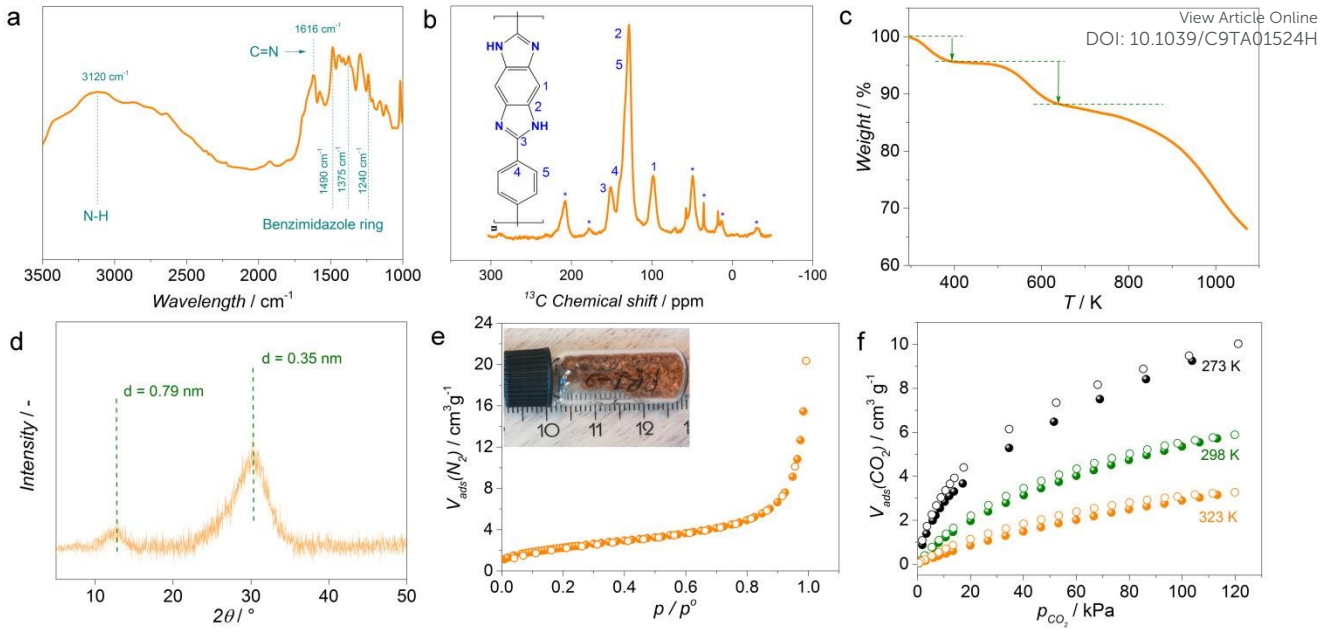

Fig. 3 Characterization of PBDI films: (a) DRIFT spectra, (b) ^{13}C CP/MAS spectra, (c) TGA profile, (d) PXRD pattern of PBDI film, (e) N_2 adsorption (closed symbols)/ desorption (open symbols) isotherm at 77 K and (f) CO_2 adsorption (closed symbols) / desorption (open symbols) isotherms at 273, 298 and 323 K. Peaks labelled with * in b were assigned to the spinning sidebands. The inset in e is the photo of PBDI film pieces in a glass sample bottle.

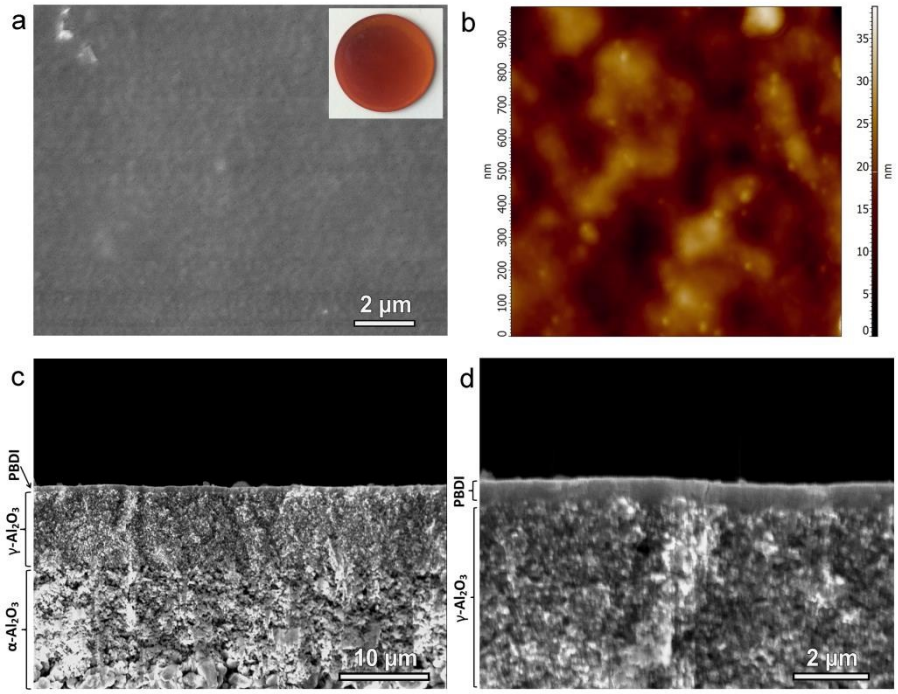

Fig. 4. SEM (a) and AFM (b) images of the membrane surface. (c) and (d) cross-section SEM images of the composite membrane. Results are obtained from M2-1.

membrane surface from the SEM and AFM images (Fig. 4a, b and Fig. S2).

3.2. Gas permeation

The reproducibility of the preparation procedure of all the three membranes (with reaction duration of 1, 2 and 3 h) was confirmed by the H_2/CO_2 separation performance at 1 bara, 373 K (Table S1).

Permeation of single gas

Before gas permeation, the as-synthesized PBDI membranes (M3-1) were on-stream activated at 373 K until a steady state was reached. The membrane was tested for permeation using H_2, CO_2, N_2, and CH_4 in single gas mode. The permeation results are provided in Table 2 and Fig. 5. The order of gas permeance roughly depends on their kinetic diameters, and there is a clearly cut-off between H_2 and the other larger gases (CO_2, N_2 and CH_4). The ideal selectivity of H_2 over CO_2, N_2 and CH_4 is 18.9, 59.7 and 47.5, respectively and

exceeds by far the corresponding Knudsen selectivity (Table 2), reflecting the formation of a dense membrane. However, the permeance does not exactly follow the order of the kinetic diameters of the measured gas molecules as exemplified by the case of CH_4. This is probably due to some preferable adsorption of CH_4 over N_2 on PBDI. Similar adsorption results had been reported for other imidazole-linked polymers.[47, 48]

Table 2. Permeances, ideal selectivities for single gas at 373 K and 1 bara feed pressure (M3-1 membrane).

Gas	Kinetic diameter (Å)	Permeance (GPU)	Ideal selectivity (H_2/-)	Knudsen selectivity
H_2	2.89	71.7	-	
CO_2	3.3	3.8	18.9	4.7
N_2	3.64	1.2	59.7	3.7
CH_4	3.76	1.5	47.5	2.8

Effect of reaction duration

Interfacial polymerization was performed at the monomer concentration of 1.5 and 1.0 wt.% for aqueous BTA and organic TPA phase, respectively. Fig. 6a presents the gas separation performance at 423 K of three membranes synthesized for 1, 2 and 3 h, respectively. Both gas permeance (H_2 and CO_2) and H_2/CO_2 selectivity increase with increasing the reaction time from 1 h to 2 h. We speculate that this is due to the fact that the unreacted monomers may block gas permeation after only 1 h reaction. Longer synthesis times would allow for more monomers to encounter the reactive functional groups, leaving more free volume for gas permeation. The gas permeance started to decrease when further increase reaction time to 3 h owing to the formation of additional layers thus increasing the thickness of the selective layer. As depicted in Fig. 4d and Fig. S4, the membrane thickness is ca. 0.60, 0.80 and 1.3 µm, corresponding to 1, 2 and 3 h reaction duration, respectively. The H_2/CO_2 selectivity seems to level off at 23 after 2 h reaction and the 2 h membrane could reach a permeance of 241 GPU.

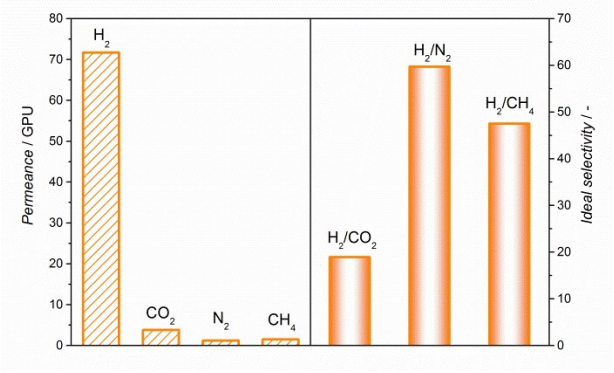

Fig. 5 Pure gas permeances of PBDI membrane at 373 K and ideal selectivity (M3-1 membrane).

Effect of feed temperature

Generally, gas transport in dense polymer membranes results from a combination of sorption and diffusion. H_2 shows high diffusion in polymer membranes owing to the smaller molecular size and CO_2 exhibits higher sorption ability because of its high condensability and polarity. The interplay between diffusion and sorption as a function of temperature can be optimized to obtain enhanced separation performance. Thus, single and mixed-gas permeation tests were performed at different temperatures to well understand the gas transport properties of PBDI membrane. Both the H_2 and CO_2 permeance of the membrane increased with increasing temperature (Fig. 6b), demonstrating an activated diffusion dominated gas transport. The effect of temperature on gas permeance (see details in SI) was captured by an Arrhenius relation. The apparent activation energy for H_2 permeation is higher than for CO_2 in both mixed and single gas permeation due to the moderating effect of the heat of adsorption for CO_2 (Fig. S6 and Table S3). The stronger influence of temperature on H_2 permeation, results in an increase in H_2/CO_2 selectivity with temperature (up to 373 K).

Effect of feed pressure

In addition to operating temperature, the effect of feed pressure (ranging from 1 to 5 bara) on both single and mixed-gas permeation were conducted at 373 K to further understand the gas transport behavior and pressure resistance of PBDI membranes. As depicted in Fig. 6c, both H_2 and CO_2 permeance decreased with feed pressure. For CO_2 this is usually attributed to an effect of non-linear adsorption, but adsorption of H_2 will be linear if any. It is

View Article Online
DOI: 10.1039/C9TA01524H

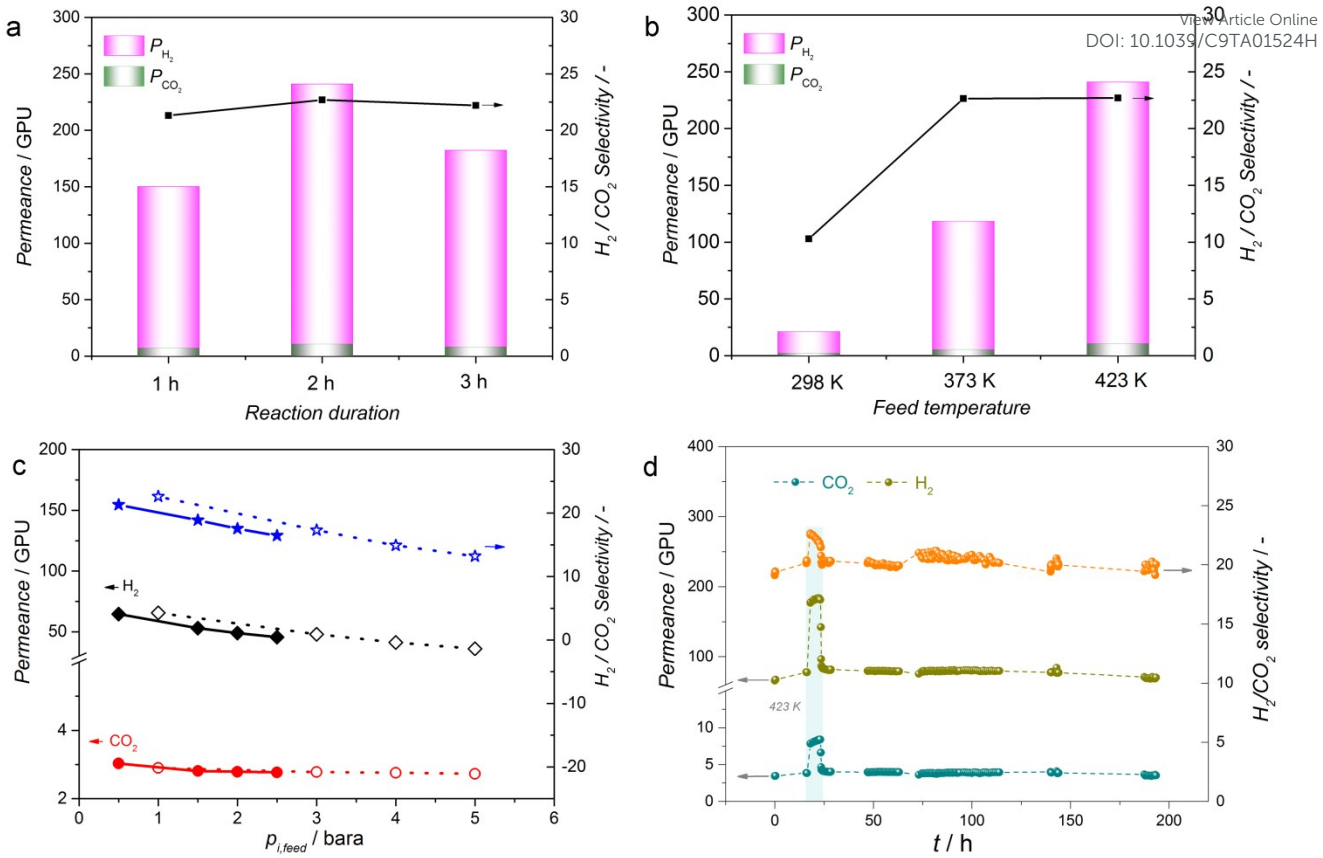

Fig. 6 Effect of (a) reaction duration (permeation at 423 K, 1 bara), (b) temperature (at 1 bara) and (c) pressure (at 373 K) on H_2/CO_2 mixture separation performance of PBDI membrane. Dashed and solid lines in (c) correspond to single component and equimolar mixed gas test, respectively. (d) Long-time stability for H_2/CO_2 separation under 373 and 423 K (blue shaded area) at 1 bara. Samples used M1-1, M2-1 and M3-1 (a), M2-1 (b), and M3-2 (c) and M3-1 (d).

interpreted that the higher feed pressure leads to a more compact packing of polymer chains.[49] Plasticization by CO_2 is therefore not observed in the studied pressure range. Compared with the single component test, H_2 permeance and selectivity slightly dropped in the mixed gas operation due to the competitive permeation of CO_2. The supported membrane was robust at 5 bara confirming a good mechanical strength.

Stability

High-performance polymeric membranes with good stability at elevated temperatures are required to realize a robust membrane system. From this point of view, the durability of PBDI membrane was examined at 373 and 423 K. The membrane can maintain the high permeance and selectivity with small fluctuation over 200 h (Fig. 6d), verifying its immutable structure and applicability for long-term use.

Comparison with literature

For comparison, the unveiled performance of membranes based on the PBI family in the configuration of flat sheet and hollow fiber are summarized in Table S4 and presented in Fig. 7a. The PBDI membranes are clearly superior to most of the state-of-the-art PBI membranes, highlighting the significance of IP protocol and the novel material. Furthermore, the potential of the PBDI membrane for real industrial application was assessed referring to the target performance region (Fig. 7a, green area). As reported,[50, 51] with a H_2 permeance >100 GPU and H_2/CO_2 selectivity >15, the environmental-friendly membrane technology can significantly reduce hydrogen production cost against the conventional cold absorption-based scrubbing processes. The performance of PBDI membrane (M2-1) with a H_2 permeance of 241 GPU and selectivity of 23, clearly located in the commercial target region, pointing out its value for real application.

View Article Online
DOI: 10.1039/C9TA01524H

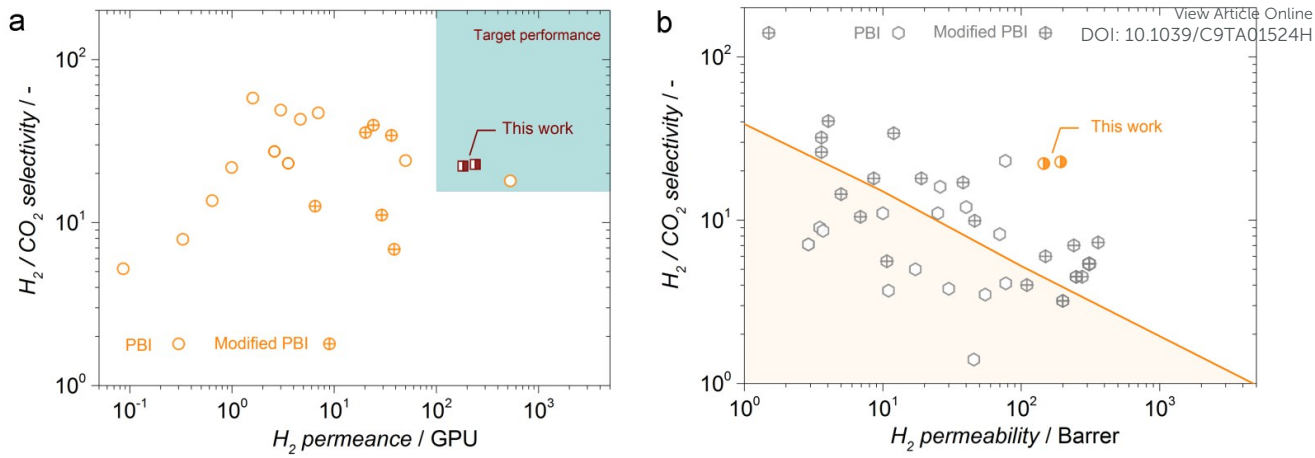

Fig. 7 (a) Comparison of H_2 permeance and H_2/CO_2 selectivity of our PBDI membranes (M2-1 and M3-1) with previously reported PBI based membranes, as well as the target performance region for pre-combustion CO_2 capture (inset green area).[50, 51] (b) Comparison of H_2 permeability and H_2/CO_2 selectivity of our membrane with previously reported polymer membranes. The 2008 Robeson bound line[52] was shown for reference. The data points were plotted referring to Table S4 and S5.

Additionally, in order to benchmark and give a general overview of the membrane material performance, the PBDI membrane thickness was used for normalization. The reported permeability of PBI and modified PBI membranes (instead of permeance) are listed (Table S5) and plotted together with the Robeson upper bound[52] (Fig. 7b). The PBDI membrane performance transcended the Robeson upper bound by a wide margin and outperformed both the PBI and modified PBI membranes, demonstrating the developed PBDI membranes possess excellent H_2 permeability and H_2/CO_2 selectivity.

4. Conclusions

In summary, free-standing PBDI films and supported PBDI membranes were successfully prepared for the first time through a facile, easy to scale up interfacial polymerization approach. Single component and mixture permeation data demonstrates a high H_2 selectivity over CO_2, N_2 and CH_4 of the membrane, reflecting the formation of a dense layer. An optimal membrane was obtained for an interfacial polymerization reaction time of 2 h, possessing an ultrahigh hydrogen permeance of 241 GPU and a H_2/CO_2 selectivity of 23 at 423 K, which overcomes the 2008 Robeson upper bound limit by a wide margin. In addition, the membrane performed stable during ~200 h at elevated temperatures and pressure. Results of an economic evaluation indicate that our membrane is located well in the target performance region and is more energy efficient than previously reported PBI membranes, demonstrating the great advantages of IP method for the preparation of defect-free PBI membranes. The appealing H_2/CO_2 separation performance, also for H_2 mixtures with N_2 and CH_4, together with such a simple fabrication method paves a way for the industrial use of membranes for H_2 purification and pre-combustion CO_2 capture.

Conflicts of interest

The authors declare that they have no competing interests except one patent application (U.S. Provisional Patent NO. 62/659, 271)

Acknowledgements

Meixia Shan gratefully acknowledge the supporting from the China Scholarship Council.

Notes and References

1. J. A. Turner, *Science*, 2004, 305, 972-974.
2. T. Yang, Y. Xiao and T.-S. Chung, *Energy & Environmental Science*, 2011, 4, 4171-4180.
3. R. Mariscal, P. Maireles-Torres, M. Ojeda, I. Sádaba and M. López Granados, *Energy & Environmental Science*, 2016, 9, 1144-1189.
4. A. Klerke, C. H. Christensen, J. K. Nørskov and T. Vegge, *Journal of Materials Chemistry*, 2008, 18, 2304-2310.
5. G. J. Stiegel and M. Ramezan, *International Journal of Coal Geology*, 2006, 65, 173-190.
6. H. Lin, E. Van Wagner, B. D. Freeman, L. G. Toy and R. P. Gupta, *Science*, 2006, 311, 639-642.
7. N. W. Ockwig and T. M. Nenoff, *Chemical Reviews*, 2007, 107, 4078-4110.
8. K. A. Berchtold, R. P. Singh, J. S. Young and K. W. Dudeck, *Journal of Membrane Science*, 2012, 415-416, 265-270.
9. B. Seoane, J. Coronas, I. Gascon, M. E. Benavides, O. Karvan, J. Caro, F. Kapteijn and J. Gascon, *Chemical Society Reviews*, 2015, 44, 2421-2454.
10. S. Wang, X. Li, H. Wu, Z. Tian, Q. Xin, G. He, D. Peng, S. Chen, Y. Yin, Z. Jiang and M. D. Guiver, *Energy & Environmental Science*, 2016, 9, 1863-1890.
11. T.-H. Bae and J. R. Long, *Energy & Environmental Science*, 2013, 6, 3565-3569.
12. S. Japip, K.-S. Liao and T.-S. Chung, *Advanced Materials*, 2017, 29, 1603833.

13. B. Zhu, C. H. Tang, H. Y. Xu, D. S. Su, J. Zhang and H. Li, *Journal of Membrane Science*, 2017, 526, 138-146.
14. J. K. Das, N. Das and S. Bandyopadhyay, *Journal of Materials Chemistry A*, 2013, 1, 4966-4973.
15. H. Li, Z. Song, X. Zhang, Y. Huang, S. Li, Y. Mao, H. J. Ploehn, Y. Bao and M. Yu, *Science*, 2013, 342, 95-98.
16. Y. Peng, Y. Li, Y. Ban, H. Jin, W. Jiao, X. Liu and W. Yang, *Science*, 2014, 346, 1356-1359.
17. X. Wang, C. Chi, K. Zhang, Y. Qian, K. M. Gupta, Z. Kang, J. Jiang and D. Zhao, *Nature Communications*, 2017, 8, 14460.
18. Z. Qiao, S. Zhao, M. Sheng, J. Wang, S. Wang, Z. Wang, C. Zhong and M. D. Guiver, *Nature Materials*, 2018, DOI: 10.1038/s41563-018-0221-3.
19. J. G. Wijmans and R. W. Baker, *Journal of Membrane Science*, 1995, 107, 1-21.
20. M. J. C. Ordoñez, K. J. Balkus, J. P. Ferraris and I. H. Musselman, *Journal of Membrane Science*, 2010, 361, 28-37.
21. D. F. Sanders, Z. P. Smith, R. Guo, L. M. Robeson, J. E. McGrath, D. R. Paul and B. D. Freeman, *Polymer*, 2013, 54, 4729-4761.
22. H. Vogel and C. S. Marvel, *Journal of Polymer Science*, 1961, 50, 511-539.
23. T. Yang and T.-S. Chung, *International Journal of Hydrogen Energy*, 2013, 38, 229-239.
24. S. S. Hosseini, N. Peng and T. S. Chung, *Journal of Membrane Science*, 2010, 349, 156-166.
25. S. C. Kumbharkar and K. Li, *Journal of Membrane Science*, 2012, 415-416, 793-800.
26. S. C. Kumbharkar and U. K. Kharul, *Journal of Membrane Science*, 2010, 357, 134-142.
27. L. Zhu, M. T. Swihart and H. Lin, *Journal of Materials Chemistry A*, 2017, 5, 19914-19923.
28. L. Zhu, M. T. Swihart and H. Lin, *Energy & Environmental Science*, 2018, 11, 94-100.
29. S. H. Han, J. E. Lee, K.-J. Lee, H. B. Park and Y. M. Lee, *Journal of Membrane Science*, 2010, 357, 143-151.
30. T. Yang, G. M. Shi and T.-S. Chung, *Advanced Energy Materials*, 2012, 2, 1358-1367.
31. J. Sánchez-Laínez, B. Zornoza, S. Friebe, J. Caro, S. Cao, A. Sabetghadam, B. Seoane, J. Gascon, F. Kapteijn, C. Le Guillouzer, G. Clet, M. Daturi, C. Téllez and J. Coronas, *Journal of Membrane Science*, 2016, 515, 45-53.
32. S. C. Kumbharkar, Y. Liu and K. Li, *Journal of Membrane Science*, 2011, 375, 231-240.
33. J. Sánchez-Laínez, B. Zornoza, C. Téllez and J. Coronas, *Journal of Membrane Science*, 2018, 563, 427-434.
34. S. Karan, Z. Jiang and A. G. Livingston, *Science*, 2015, 348, 1347-1351.
35. B.-H. Jeong, E. M. V. Hoek, Y. Yan, A. Subramani, X. Huang, G. Hurwitz, A. K. Ghosh and A. Jawor, *Journal of Membrane Science*, 2007, 294, 1-7.
36. M. J. T. Raaijmakers and N. E. Benes, *Progress in Polymer Science*, 2016, 63, 86-142.
37. M. F. Jimenez-Solomon, Q. Song, K. E. Jelfs, M. Munoz-Ibanez and A. G. Livingston, *Nature Materials*, 2016, 15, 760.
38. S. Lin and L. Yang, *Tetrahedron Letters*, 2005, 46, 4315-4319.
39. D. W. Tomlin, A. V. Fratini, M. Hunsaker and W. Wade Adams, *Polymer*, 2000, 41, 9003-9010.
40. S. Li, J. R. Fried, J. Colebrook and J. Burkhardt, *Polymer*, 2010, 51, 5640-5648.
41. M. Shan, X. Liu, X. Wang, I. Yarulina, B. Seoane, F. Kapteijn and J. Gascon, *Science Advances*, 2018, 4, eaau1698.
42. P. Totsatitpaisan, S. P. Nunes, K. Tashiro and S. Chirachanchai, *Solid State Ionics*, 2009, 180, 738-745.
43. J. Yang and R. He, *Polymers for Advanced Technologies*, 2010, 21, 874-880.
44. S. Jenkins, K. I. Jacob, M. B. Polk, S. Kumar, T. D. Dang and F. E. Arnold, *Macromolecules*, 2000, 33, 8731-8738.
45. A. K. Sekizkardes, S. Altarawneh, Z. Kahveci, T. İslamoğlu and H. M. El-Kaderi, *Macromolecules*, 2014, 47, 8328-8334.
46. A. K. Sekizkardes, J. T. Culp, T. Islamoglu, A. Marti, D. Hopkinson, C. Myers, H. M. El-Kaderi and H. B. Nulwala, *Chemical Communications*, 2015, 51, 13393-13396.
47. S. C. Kumbharkar, P. B. Karadkar and U. K. Kharul, *Journal of Membrane Science*, 2006, 286, 161-169.
48. M. G. Rabbani and H. M. El-Kaderi, *Chemistry of Materials*, 2012, 24, 1511-1517.
49. A. Ebadi Amooghin, M. Omidkhah and A. Kargari, *RSC Advances*, 2015, 5, 8552-8565.
50. T. C. Merkel, M. Zhou and R. W. Baker, *Journal of Membrane Science*, 2012, 389, 441-450.
51. L. Giordano, J. Gubis, G. Bierman and F. Kapteijn, *Journal of Membrane Science*, 2018, DOI: https://doi.org/10.1016/j.memsci.2018.12.063.
52. L. M. Robeson, *Journal of Membrane Science*, 2008, 320, 390-400.

View Article Online
DOI: 10.1039/C9TA01524H

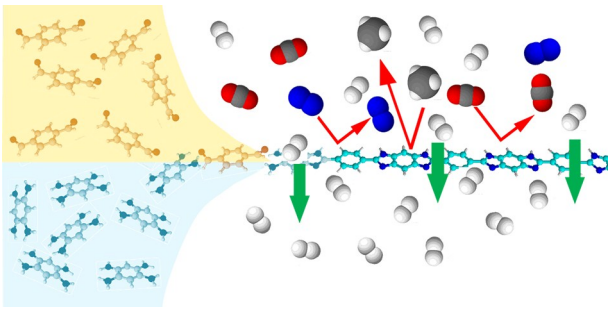

Novel polybenzimidazole PBDI membranes with ultrahigh H_2 separation performance were developed by a facile interfacial polymerization approach.